Available online at www.sciencedirect.com

SciVerse ScienceDirect

journal homepage: www.elsevier.com/locate/jmbbm

Research paper

Single and reciprocal friction testing of micropatterned surfaces for orthopedic device design

N. Mitchell[a], C. Eljach[b], B. Lodge[a], J.L. Sharp[c], J.D. DesJardins[b], M.S. Kennedy[a,*]

[a] School of Materials Science and Engineering, Clemson University, Clemson, SC 29634, United States
[b] Department of Bioengineering, Clemson University, Clemson, SC 29634, United States
[c] Department of Mathematical Sciences, Clemson University, Clemson, SC 29634, United States

ARTICLE INFO

Article history:
Published online 16 September 2011

Keywords:
Surface engineering
Friction
Lubricated
Reciprocating

ABSTRACT

The use of micropatterning to create uniform surface morphologies has been cited as yielding improvements in the coefficient of friction during high velocity sliding contact. Studies have not been preformed to determine if these micropatterns could also be useful in biomedical applications, such as total joint replacement surfaces, where the lower sliding velocities are used. In addition, other factors such as lubricant viscosities and materials used are more tightly constrained. In this study, the effect of pattern geometry, feature size and lubricant on contact friction and surface damage was investigated using 316L steel in sliding contact with a stainless steel and polyethylene pins. Using a novel proprietary forming process that creates millions of microstructures in parallel, a variety of micropatterned surfaces were fabricated to study the influence of shape (oval, circular, square), geometry (depressions, pillars) and feature size (10, 50 and 100 mm) on both contact friction and surface damage. All samples were 316L stainless steel and the static and dynamic coefficients of friction when in contact with either a stainless steel or polyethylene counterface were measured in dry and lubricated conditions. All samples were characterized for surface uniformity and pattern aspect ratio using white light interferometry and optical microscope image analysis, and the coefficients of friction were measured for each surface/lubricant/pin system using a CETR scratch testing system. Results showed that round depressions with diameters of 10 μm had a significantly lower steady state coefficient of friction than the non-patterned substrates or substrates with greater diameter depression patterns. In addition, our results showed that the single-pass coefficient of friction measurements were not good predictors of the steady state coefficient of friction values measured.

© 2011 Elsevier Ltd. All rights reserved.

1. Introduction

The wear and sliding resistance of both metal–metal contact (hip joints and bushings) and metal–polymer contact (hip/knee/spine joints and journal bearings) are of critical importance to artificial joint function. With even minor changes in joint coefficient of friction (CoF), the compressive loads developed across a human joint can result in

* *Corresponding author.* Tel.: +1 864 656 5349.
E-mail address: mskenne@clemson.edu (M.S. Kennedy).

1751-6161/$ - see front matter © 2011 Elsevier Ltd. All rights reserved.
doi:10.1016/j.jmbbm.2011.08.022

insufficient patient muscle forces to effectively initiate joint motion. Artificial joint replacement procedures are major operations that are both costly and painful. Because they require intensive post-operative therapy, it is hoped that the lifetime of the joint will exceed the lifetime of the patient. This lifetime is directly proportional to the wear of the bearing material. As in other applications, total joint replacement bearing materials have the potential to be improved through the use of micropatterned surfaces. The literature has shown that both uniform and non-uniform micropatterned surfaces (Nakano et al., 2007; Pettersson and Jacobson, 2004; VanDamme et al., 2003) led to an improvement in the tribological properties during sliding contact and supports the use of micropatterned surfaces in bearing applications. By placing uniform, small, localized depressions into smooth regions of sliding surfaces, researchers have shown they can change the sliding CoF. Studies attribute these improvements to the ability of these depressions to act as either lubricant reservoirs or traps for wear particles. In addition, the studies of VanDamme et al. (2003) also highlight the ability of non-uniform patterns to change the CoF in orthopedic devices. Also, using shot peening to create "craters" in the surface, Nakano et al. (2007) reported a decrease in the frictional coefficient during lubricated sliding contact. The advantage of the uniform patterning is a consistent decrease in the CoF's measured deviation when compared to untreated surfaces.

Friction and wear are the result of physical interactions between two materials as they slide over each other. These interactions are influenced by the type of material, the geometrical and topographical characteristics of the surfaces, the applied load, and the environmental conditions under which the surfaces are made to slide against each other (Axen et al., 2000). Friction and wear in biomaterials occur under challenging environmental conditions without the ability to service or artificially lubricate the system. As such, only a limited number of biomaterials have been determined to be suitable for long-term use in total joint replacements. The use of surface micropatterning in total joint replacement biomaterials adds an additional level of bearing design that can influence friction and wear, without sacrificing the use of accepted biomaterials.

One specific advantage of the micropatterned surface is that it provides multiple reservoirs for lubricant. The available lubricant decreases the friction forces and provides possible localized hydrodynamic effects. Without micropatterning or inherent roughness, lubricant can be more easily removed from the system during sliding. Surface micropatterning retains lubricant at the points of contact (Blatter et al., 1999; Kononenko et al., 2000; Pettersson and Jacobson, 2007, 2003; Ryk et al., 2002). This also stabilizes the fluctuation of the friction forces exhibited during testing. Surface micropatterning has also been shown to improve tribological properties because particles from wear damage can be trapped, which reduces the plowing mechanism (Pettersson and Jacobson, 2003; Dumitru et al., 2003; Saka et al., 1989; Suh et al., 1994; Suh and Saka, 1987; Tian et al., 1989). Reduction in the plowing mechanism prolongs both the life of the lubricant and minimizes the amount of deformation during sliding contact. Micropatterns have been shown to act as "interrupts" of surface deformation, restricting local contact area growth through trapping the wear particles and locally supplying sufficient lubrication within the contact area (Pettersson and Jacobson, 2007). Such depressions can also reduce the coefficient of friction by 90% (Nakano et al., 2007) due to the increased area of the hydrodynamic lubrication regime (Dumitru et al., 2000). Another micropatterning variable that drastically affects the CoF is the density of the pattern. It has been previously shown that as the depression density increases, the coefficient of friction decreases (Kligerman et al., 2005). In contrast, grooves have been shown to increase the coefficient of friction by approximately 30% (Kononenko et al., 2000), perhaps due to the suppression of the hydrodynamic lubrication regime, resulting in boundary lubrication regimes.

One of the greatest challenges to using micropatterning for total joint replacements is the ability to inexpensively and uniformly pattern the surfaces. We investigated the patterns produced from a novel parallel patterning process for use on a model artificial joint biomaterial—316L stainless steel. Today the most common material for articulating surfaces in artificial joints are CoCrMo or ceramics, but we used 316L stainless steel as a trial material for this proof-of-concept study on the surface micropatterning. We hypothesize that micropatterning will show a beneficial lowering of the CoF for this model material.

2. Experimental details

2.1. *Equipment*

The tribological experiments were performed using either a ball-on-flat or flat-on-flat reciprocating set up. The linear scratch-testing unit used during testing was a CETR UMT-2 (Center for Tribology Inc., Campbell, CA) microscratch system with a 20 N bi-axial load cell (Fig. 1). A cantilevered suspension attachment was used to maintain uniform loading of the counterface tip. All tests were performed at room temperature at a normal load of 15 N, a pin velocity of 10 mm/s, and a 2 cm sliding contact path length. The mean surface pressure for each system is listed in Table 1 and calculated using the available bearing peak surface areas provided by the micropatterned surfaces. For the ball bearing, the mean pressure was determined using a Hertzian contact.

2.2. *Specimens*

2.2.1. *Preparation and characterization of steel coupons used as the lower specimens*

Eight micropatterned samples, containing either depressions or pillars (Fig. 2), were fabricated at Hoowaki LLC (Pendleton, SC) using a proprietary surface forming process. These samples are listed in Table 1. There were two shapes of depressions: circular and oval, and three shapes of pillars: circle, oval, and square. Non-patterned 316L stainless-steel samples were also fabricated as a control surface.

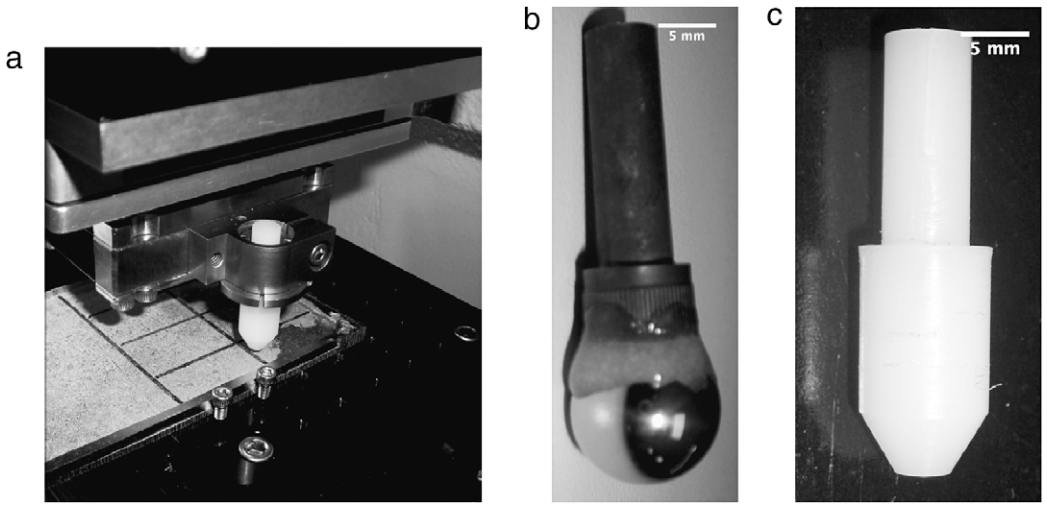

Fig. 1 – CETR system (a) with metallic ball (b) and polymer flat pins (c) used for testing.

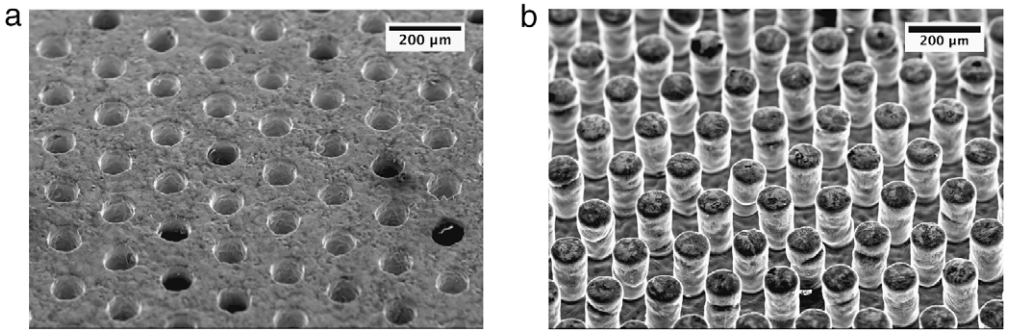

Fig. 2 – SEM image showing the surface micropatterning of 100 μm circular holes (a) and 100 μm circular pillars (b).

2.2.2. *Preparation and characterization of pins used as the upper specimens*

Two different types of counterface pins were used: a 12.7 mm diameter chrome steel ball bearing (AISI 52100), and a conical shaped, 4 mm diameter flat surface polyethylene pin (UHMWPE GUR 1020) (Fig. 1). Before testing, the surface roughness average of each chrome-stainless steel ball bearing and the polyethylene pin were measured using a non-contact white light surface interferometer (WYKO NT-2000, Veeco, Inc. Tucson, AZ).

2.2.3. *Lubricants*

These samples were first tested under dry conditions, and then later tested using Cannon Instrument Company N35 viscosity standard, a highly refined mineral oil. This mineral oil was chosen as a lubricant because its rheological properties are similar to the lubricant viscosity of degenerated human synovial fluid—specifically a kinematic viscosity of 66cP, which is within the range of degenerated human synovial fluid shown by Schurz and Ribitsch (1987).

2.3. *Experiment procedures*

All tests were conducted with a normal load of 15 N, pin velocity of 10 mm/s, and a 2 cm sliding contact path length. These samples were first tested under dry conditions with no lubrication. Next, the same specimens were then tested at a different location using N35 mineral oil as a lubricant. The first was a single pass test (sliding contact in one direction for 2 cm) using the parameters mentioned before. The second was a reciprocating test, which moved the pin over the sample a total of 50 cycles. With one cycle being two passes, one down and one back along the same motion path. Testing parameters remained as before (15 N, 10 mm/s, 2 cm travel). A surface roughness measurement of the ball bearing was taken after each single pass and reciprocal sliding test to determine if there was damage to the counterface surface. The reported surface roughness was the arithmetic average roughness. Vickers tests were performed after reciprocal pass tests to measure damage track hardness changes.

2.3.1. *Single pass CoF testing*

Using the testing parameters from above, the dynamic CoF along the length of the single pass was measured. The static coefficient of friction was not considered for this measurement, with steady state requiring approximately 0.25 s to attain. A sample of these data can be seen in Fig. 3.

Table 1 – Micropatterned samples provided by Hoowaki LLC.

Surface type	Feature geometry	Feature measured	Feature size (μm) (Average ±1 StD.)	Height or depth (μm)	Aspect ratio (height:width)	Bearing surface area (%)	Ball bearing mean surface pressure (MPa)	Polyethylene pin mean surface pressure (MPa)
Flat				±			396.0	1.2
Depressions	Round	Diameter	10.99 ± 3.19	5.41 ± 1.66	0.49	68.9	574.4	1.7
	Round	Diameter	50.81 ± 0.84	26.13 ± 0.67	0.53	72.8	544.2	1.6
	Round	Diameter	99.77 ± 1.26	77.90 ± 2.89	0.79	71.2	556.0	1.7
	Oval	Short side	18.70 ± 1.29	58.01 ± 2.28	1.53	74.8	529.7	1.6
		Long side	38.03 ± 3.77					
Pillars	Round	Diameter	50.73 ± 0.94	18.35 ± 1.67	0.36	28.2	1402.4	4.2
	Round	Diameter	96.55 ± 6.71	139.00 ± 0.95	0.49	30.2	1311.0	4.0
	Oval	Short side	18.50 ± 3.35	56.54 ± 1.54	1.49	12.1	3286.4	9.9
		Long side	37.70 ± 2.43					
	Square	Side	17.80 ± 1.35	66.81 ± 2.64	1.43	32.7	1212.4	3.7

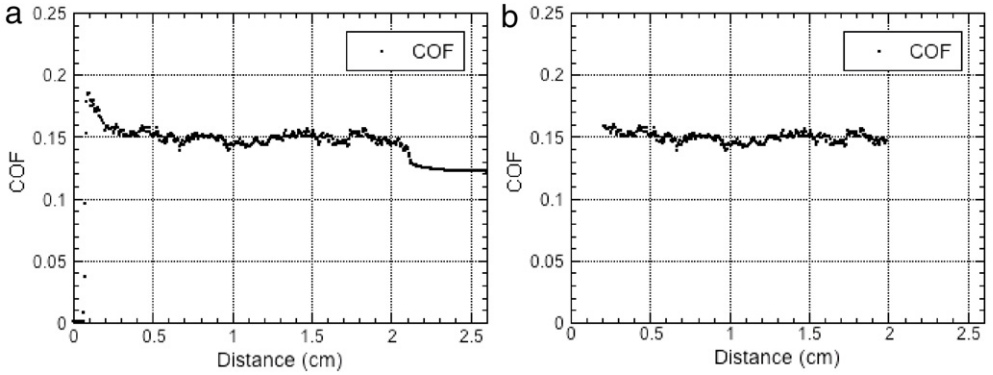

Fig. 3 – Data processing for the single pass friction tests. The first 0.25 s are not taken into consideration for the friction measurement. The raw data (a) is then transformed into the processed data (b).

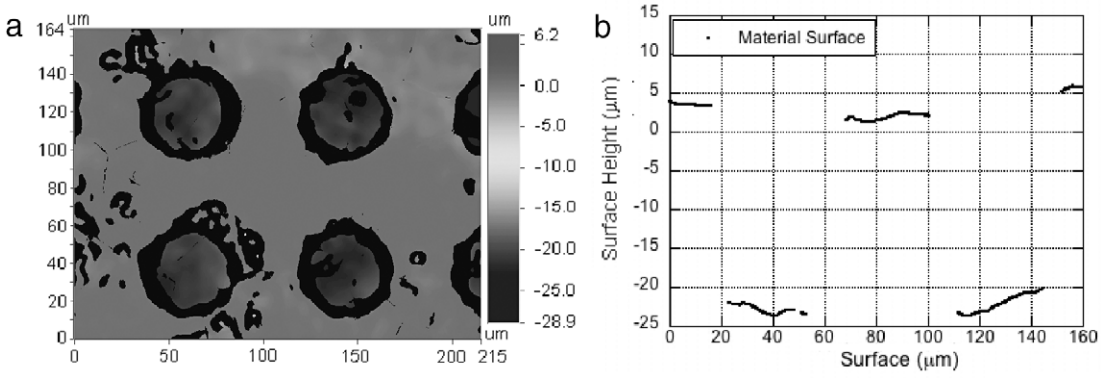

Fig. 4 – Non-contact surface topography analysis was used to determine the feature aspect ratio (width vs. depth) (50 μm depression pattern shown). (a) shows the topography surface plot and (b) shows a cross sectional measurement.

2.3.2. *Reciprocal pass testing*

Using the same parameters of the single pass testing, reciprocal sliding tests were performed on the micropatterned samples. Using the same idea as in the single pass CoF testing, the first 0.25 s was not considered for the dynamic CoF. Also, since the pin stops and reverses direction, additional data processing was considered for each data cycle. Every time the pin halted and changed direction, data 0.1 s before and after the pin stopped was not considered for the dynamic CoF measurement. Once the system reached a steady state, the cycles 30–50 were used in the calculation of the steady state values and standard deviations.

2.4. *Statistical analysis*

Statistical analyses were conducted using SAS v. 9.2. SAS Institute Inc. (2008). Within the lubricated and dry samples, factorial analysis of variance (ANOVA) was conducted for the initial coefficient of friction with two levels of pattern (depressed and pillar) with common geometries and feature size (oval with feature size 25 × 50, round with feature size 50, and round with feature size 100). Follow-up analyses were conducted using Fisher's Least Significant Difference. Factorial analysis was not conducted with the samples without a pattern, a feature size of 10, or a square geometry, as these were not common to all patterns and geometries. Replicates were not obtained for steady state coefficient of friction, so factorial ANOVA was not conducted. Significance was established with $\alpha = 0.05$.

3. Results

3.1. *Sample geometry*

Sample micropattern geometry was measured with a Veeco white light interferometer (±0.1 nm surface height resolution) and an optical microscope with image analysis software. The feature-defining dimensions (circle diameter, square side length or oval diameters) were measured in addition to the feature height (pillars) or depth (depressions). An example of the characterization of round depressions and the surface feature dimensions is shown in Figs. 4 and 5. Using the height and width, the aspect ratio of each pattern was determined. The bearing (contact) surface area is a ratio of the area in contact with the ball on the micropatterned surface as compared to that of a non-patterned surface, which is different for each micropattern due to different feature size and feature density. This bearing surface area will change as the ball bearing pin wears into the material, due to it being a non-conformal counterface. A summary of the dimensions, aspect ratios and contact area for each pattern is summarized in Table 1.

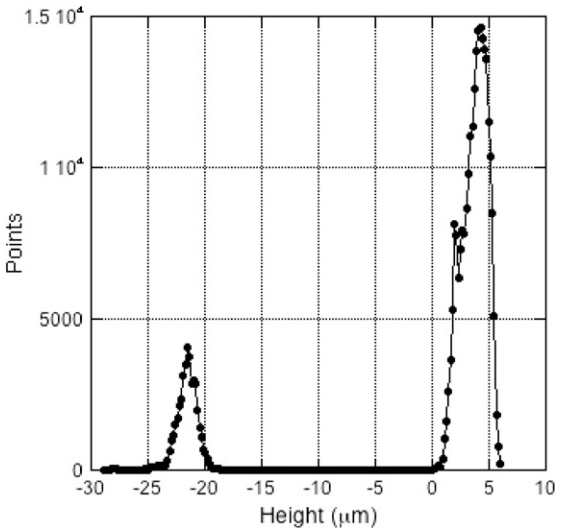

Fig. 5 – Non-contact surface topography analysis (surface histogram) to determine bi-modal surface feature height (and thus average feature height/depth) (50 μm depression pattern shown). Distance between peaks is depth/height measurement.

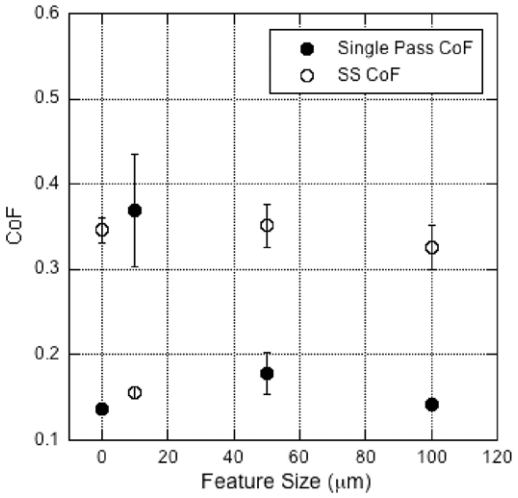

Fig. 6 – The round depression diameter influences the initial CoF, but more importantly it shows that this initial CoF is not an indicator of the SS CoF for the ball bearings. The non-patterned samples are shown as zero feature size.

3.2. *Single pass CoF tests*

3.2.1. *Ball bearing*

Non-patterned 316L samples (controls) had an initial single pass CoF of 0.15 ± 0.01 and a steady state (SS) coefficient of friction of 0.16 ± 0.02 as shown in Fig. 6. As the diameter increased in the micropatterned circular depressions, the coefficient of friction decreased for the dry and lubricated tests. The opposite behavior was seen in the pillars: as the pillar size increased, the coefficient of friction decreased in the lubricated tests. Under dry conditions, however, little difference was observed. As the bearing area increased, the coefficient of friction decreased for both lubricated and non-lubricated conditions for the micropatterned depressions. A similar pattern was seen with the pillars—as the bearing area increased, the coefficient of friction decreased. The lowest observed coefficient of friction was from the 25 μm × 50 μm oval depressions under both lubricated and non-lubricated conditions. The coefficients of friction for both the 10 and 50 μm circular depressions increased with the addition of the N35 mineral oil lubricant, while the coefficient of friction for the 25 μm × 50 μm oval depressions decreased with the addition of lubricant. The coefficients of friction for the 50 μm circular pillars, 25 μm square pillars, and 25 μm × 50 μm oval pillars all increased with the addition of lubricant, while the coefficient of friction for the 100 μm circular depressions decreased with the addition of lubricant. Optical images of the micropatterned surfaces showed abrasion after one cycle and 50 cycles, as shown in Fig. 7. All ball bearing surfaces showed significant scratching after reciprocating sliding against the patterned and non-patterned surfaces. Material adhesion on the ball bearings was also evident, and was observed to change depending on the type of feature that was present; the pillars showed more adhesion than the depressions.

3.2.2. *Polyethylene pin*

When the polyethylene pin articulated against the patterned surfaces, as the depression size increased, the coefficient of friction decreased under both lubricated and non-lubricated conditions. For the pillars, the coefficient of friction decreased with increasing pillar size. Similar to the ball bearing test, the surface bearing area affected the coefficient of friction; as the surface bearing area increased, the coefficient of friction decreased.

3.3. *Statistical analysis results*

For both dry and lubricated tests, significant interactions existed between patterns and feature sizes within geometries ($F(2, 2200) = 949.65$, $p < 0.0001$ and $F(2, 2225) = 3137.72$, $p < 0.0001$, respectively). For the dry tests, the initial coefficient of friction for the depressed pattern with a diameter of 50 μm significantly differed from the pillar pattern with the same feature size ($p < 0.0001$), although this difference was not significant for the lubricated tests ($p = 0.8957$). The dry depressed pattern with feature size of 50 μm did not significantly differ from pillars with feature size of 100 μm ($p = 0.2709$). The average initial coefficient of friction for the pillar pattern with a feature size of 25 μm × 50 μm was significantly higher than pillars with feature sizes of 50 and 100 μm, as well as for any of the feature sizes for the depressed pattern for the dry and lubricated tests.

For both lubricated and dry tests, there were significant differences in the initial coefficient of friction among no pattern, depressions, and pillars ($F(2, 3255) = 106.35, P < 0.0001$ and $F(2, 3236) = 100.90$, $P < 0.0001$), regardless of feature size and feature geometry.

3.4. *Reciprocal pass tests*

3.4.1. *Ball bearing*

Under both non-lubricated and lubricated conditions, the steady state coefficient of friction decreased as depression

Table 2 – The initial CoF and SS CoF for all the ball bearing- micropatterned surfaces are shown below. These tests were run without a lubricant.

Depression or pillar	Feature geometry and dimensions	Initial CoF (1Pass)-no lubricant	SS CoF-no lubricant	Cycles to SS
No pattern	–	0.146 ± 0.010	0.157 ± 0.017	0
Depressions	Round (11 μm)	0.210 ± 0.030	0.129 ± 0.009	27.1
	Round (51 μm)	0.161 ± 0.021	0.490 ± 0.053	4.5
	Round (100 μm)	0.145 ± 0.011	0.543 ± 0.028	6.9
	Oval (19 × 38 μm)	0.133 ± 0.005	0.500 ± 0.051	2.8
Pillars	Round (51 μm)	0.153 ± 0.017	0.446 ± 0.034	6.2
	Round (97 μm)	0.160 ± 0.017	0.408 ± 0.049	13.7
	Oval (19 × 37 μm)	0.169 ± 0.008	0.140 ± 0.007	16.9
	Square (18 μm)	0.190 ± 0.015	0.501 ± 0.037	11.3

Table 3 – Significant changes of the CoF can be seen when a lubricant is used. This table summarizes the initial and SS CoF for the ball bearing—micropatterns.

Depressions or pillars	Feature geometry and dimensions	Initial CoF (1Pass)-lubricant used	SS CoF-lubricant used	Cycles to SS
No pattern	–	0.137 ± 0.007	0.346 ± 0.015	9.2
Depressions	Round (11 μm)	0.369 ± 0.066	0.156 ± 0.007	30.8
	Round (51 μm)	0.178 ± 0.024	0.351 ± 0.025	1.5
	Round (100 μm)	0.141 ± 0.006	0.325 ± 0.026	11.4
	Oval (19 × 38 μm)	0.12 ± 0.005	0.360 ± 0.019	2.7
Pillars	Round (51 μm)	0.178 ± 0.019	0.366 ± 0.033	2
	Round (97 μm)	0.149 ± 0.004	0.332 ± 0.019	25.5
	Oval (19 × 37 μm)	0.259 ± 0.034	0.453 ± 0.070	11
	Square (18 μm)	0.193 ± 0.009	0.296 ± 0.042	4

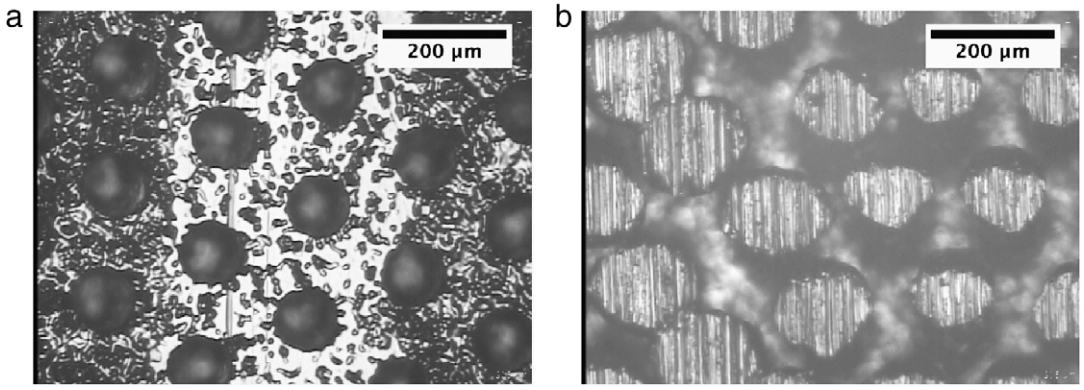

Fig. 7 – Optical images of the micropatterned surface show abrasion occurring after both one cycle and 50 cycles. (a) Damage track from single pass non-lubricated 100 μm depressions (4×, 604 × 805 μm field of view). (b) Damage track from reciprocating (50 cycles) lubricated 100 μm circular pillars (4×, 604 × 805 μm field of view).

size decreased (Tables 2 and 3). A graph representative of the depression data is shown in Fig. 8. An opposite trend was seen with the circular pillars however. Under both non-lubricated and lubricated conditions the steady state coefficient of friction decreased as pillar size increased. Under non-lubricated and lubricated conditions, the steady state coefficient of friction for the pillars decreased as the surface bearing area decreased for micropatterned depressions. Under non-lubricated and lubricated conditions the steady state coefficient of pillar friction decreased as the surface bearing area increased.

For surfaces with lower measured steady state coefficients of friction, the cross section of the damage track was narrower, and finer grooves within the damage track were also observed. The tests with lower steady state coefficients of friction had a lower Vickers hardness as shown in Table 4. For some patterns, the N35 lubricant seemed to degrade the tribological properties on the 316L stainless steel, such as seen in Tables 2 and 3 with the smooth (control) sample and with the 25 μm × 50 μm oval pillars. Dark brown areas, observed on the 25 μm × 50 μm oval pillars under non-lubricated conditions, were not observed under lubricated conditions. The surface of the ball bearing after the reciprocal pass tests was rougher, as compared to the single pass test.

Table 4 – The hardness of samples can alter after friction or abrasion testing. This alteration was tracked using a Vickers Hardness test in the damage tracks. This table shows the alteration of sample hardness as a function of the abrasion testing and lubrication.

Samples	VH-As received	VH-after testing using lubricated conditions	VH-after testing using dry conditions
	Avg ± StD	Avg ± StD	Avg ± StD
No pattern	111.5 ± 8.1	312.0 ± 19.3	139.7 ± 6.6
Round depressions (11 μm)	115.6 ± 12.5	206.8 ± 9.1	221.0 ± 8.1
Round depressions (51 μm)	109.5 ± 10.3	329.8 ± 79.6	339.8 ± 34.8
Round depressions (100 μm)	113.5 ± 4.2	260.9 ± 21.4	219.4 ± 55.7
Oval depressions (19 × 38 μm)	108.8 ± 4.9	310.8 ± 10.9	335.7 ± 95.4

Table 5 – The initial CoF and SS CoF for all the polyethylene tips—micropatterned surfaces are shown below. These tests were run without a lubricant.

Depression or pillar	Feature geometry and dimensions	Initial CoF (1Pass)-no lubricant	SS CoF-no lubricant
No pattern	–	0.073 ± 0.006	0.083 ± 0.008
Depressions	Round (11 μm)	0.214 ± 0.019	0.213 ± 0.022
	Round (51 μm)	0.132 ± 0.004	0.110 ± 0.009
Pillars	Round (51 μm)	0.167 ± 0.007	0.171 ± 0.018
	Round (97 μm)	0.168 ± 0.10	0.126 ± 0.017

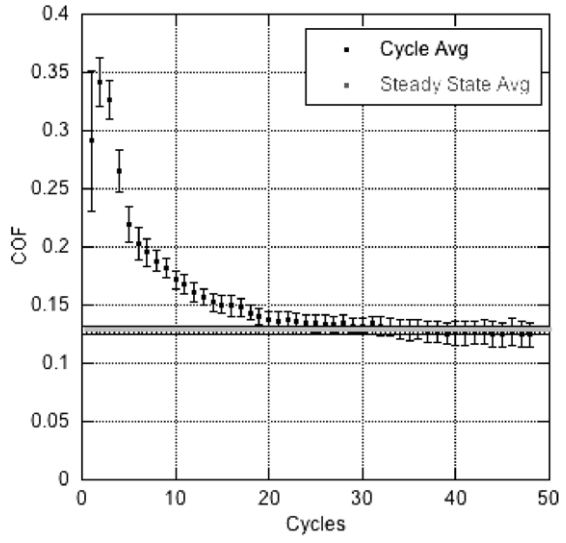

Fig. 8 – Graph comparing the coefficient of friction to the number of cycles for the non-lubricated 10 μm depressions sample. Each cycle distance is 4 cm.

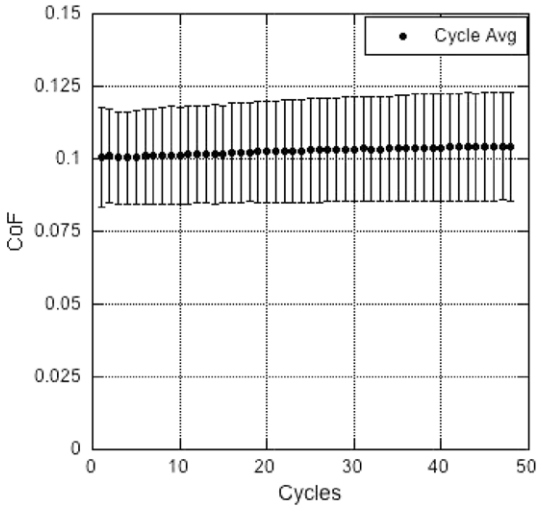

Fig. 9 – Graph showing lubricated polyethylene tip sliding over 50 μm depressions. The CoF is shown to increase slightly over time. Each cycle distance is 4 cm.

3.4.2. *Polyethylene tests*

The coefficient of friction decreased as the depression size increased Tables 5 and 6 under both lubricated and non-lubricated condition, with the pillars showing a similar trend under both lubricated and non-lubricated conditions. As pillar size increased the coefficient of friction decreased. Fig. 9 shows a slight increase in the CoF over time, which is the general trend seen with PE pins. While there was no significant damage to the micropatterned surface, more severe damage was observed on the polyethylene pin. This damage was not quantified.

3.5. *Tip assessment*

The roughness increased for each of the steel pins in contact with the surfaces during both single and reciprocal pass testing. A summary of the increases is shown in Fig. 10. As expected, under dry and lubricated conditions, reciprocal sliding produced a greater increases in counterface surface roughness than did single pass tests. Depressions under dry conditions produced a greater increase in counterface surface roughness than did pillars under dry conditions during reciprocal testing. The greatest increase in counterface surface roughness was produced from the flat surfaces with no micropatterning during reciprocal sliding.

Table 6 – The initial CoF and SS CoF for all of the polyethylene tips used on micropatterned surfaces with lubrication are shown below. There were significant changes to the depression patterns, but there was an increase in the friction seen in the pillars.

Depression or pillar	Feature geometry and dimensions	Initial CoF (1Pass)-lubricant used	SS CoF-lubricant used
No pattern	–	0.070 ± 0.01	0.08 ± 0.010
Depressions	Round (11 μm)	0.156 ± 0.045	0.201 ± 0.023
	Round (51 μm)	0.103 ± 0.007	0.104 ± 0.018
Pillars	Round (51 μm)	0.204 ± 0.032	0.194 ± 0.032
	Round (97 μm)	0.127 ± 0.011	0.1329 ± 0.017

4. Discussion

Reducing the coefficient of friction will increase their useful service life for most articulating surfaces. It is especially desirable to lengthen the lifespan of artificial joints within patients since replacement of these materials requires a costly revision surgery. The focus of this study was to investigate methods to reduce the coefficient of friction in artificial joint materials with tailored surface micro-architectures.

In the single pass ball bearing tests, it was observed that an increase in micro-architecture hole size diameter resulted in a corresponding decrease in the coefficient of friction. This inverse relationship could be hypothesized to occur because of an increase in available lubricant reservoir volume within these holes as the hole size diameter increases. In addition, these increased hole diameters could provide locations for wear particulate to be removed from 3rd body articulation. The single pass polyethylene tests also showed decreases in the coefficient of friction with increasing micro-architecture hole size diameter, which strengthens the hypothesis that a greater volume of available lubricant within these holes could provide enhanced lubrication mechanisms within this tribological system.

The addition of the polyethylene pins to this study allowed the additional examination of these metal micro-architectures on a hard–soft tribosystem similar to artificial joint replacements. These polyethylene pin tips were flat so as to better model the in vivo contact stresses and lubrication mechanisms of the sliding surfaces. In the single pass tests, the pillar diameters above 50 μm did not affect the coefficients of friction. It could be hypothesized that the greater available polyethylene surface area was a greater influence on resulting coefficient of friction than the change in micro-architecture with the pillar surfaces tested in this study.

The 100 μm circular pillars had a steady-state coefficient of friction lower than that of the 50 μm circular pillars, which could be hypothesized to be the result of the chrome balls wearing through the pattern on the 50 μm circular pillar samples. The damage track for the lubricated 100 μm circular pillars had a mirror-like finish, while the mirror-like finish did not appear in either the lubricated or non-lubricated conditions for the 50 μm circular pillar samples. This mirror-like finish, observed in similar research, has been shown to be associated with very low CoF (Suh, 1981). The reddish brown areas observed on the non-lubricated 25 μm × 50 μm pillars and non-lubricated non-patterned surfaces are hypothesized to be an oxide or a hydroxide layer that formed upon the pillar surfaces. This was also seen by other groups using 316L stainless steel (Smith, 1985) under sliding contact. Under lubricated conditions there is likely a cooling effect and with an absence of available oxygen, lubricant shielding could be hypothesized to obviate any oxidizing surface reactions. The oxide layer on the non-lubricated samples possibly formed due to frictional heating and the presence of an oxygen-rich environment, such as air. This layer could have also formed by the wearing away of the Cr oxides in stainless steel, which would allow non-oxidized metal to react with the oxygen in the air.

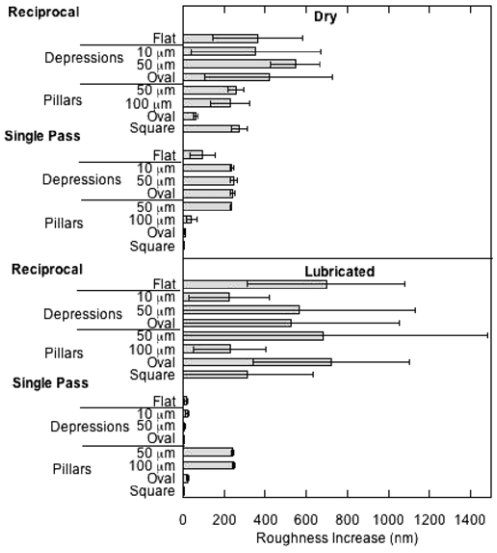

Fig. 10 – The roughness of all the steel ball pins initially had a roughness of approximately 18 nm. This plot shows the roughness increase of the bearing surface after testing.

The differential hardness of the metal before and after the reciprocal pass tests can be used to correlate how much plastic deformation has occurred. The lower Vickers hardness values after testing were characteristic of samples with lower coefficients of friction. The mirror-like surfaces had lower hardness values and narrower damage tracks because less plastic deformation occurred due to the prohibited plowing mechanism.

The results of the studies with 316L stainless steel showed that the micropatterns developed can reduce the CoF. Studies with micropatterned CoCrMo and Ti6Al4V artificial joint materials are planned for the next phase of this research.

5. Conclusions

Stainless steel balls and flat polyethylene pins articulating against 316L stainless steel plates with different micropatterns formed onto their surfaces were investigated in this study. The frictional behavior was found to strongly depend upon the size and shape of the micropatterned surfaces. Four different relationships between the articulating materials and the geometries of the surface micropatterns were observed during testing: (1) Single-pass metal ball articulation over circular surface micropatterned geometries yielded lower coefficients of friction with larger depression sizes and larger pillar sizes. (2) A single-pass polyethylene pin articulation over circular geometries yielded lower coefficients of friction with larger depression sizes. (3) Reciprocating pass testing of ball bearings over circular geometries yielded lower coefficients of friction with smaller depression sizes and larger pillar sizes. (4) Reciprocating pass testing of polyethylene pins over circular geometries yielded lower coefficients of friction with larger depression sizes and larger pillar sizes. In all cases the plowing and adhesive damage mechanisms are the most dominant types of surface damage, when analyzing the damage tracks and the counterface pins. These positive results provide the basis to continue this work with other artificial joint articulating materials.

Acknowledgments

Samples for this work were supplied by Hoowaki LLC. and the research was supported by the Clemson University Creative Inquiry program. The authors also wish to acknowledge Dr. Andrew H. Cannon for his valuable insights in the production of this paper and contribution of SEM images. In addition, the editorial assistance of Mr. G. Kimball at the Clemson University as much appreciated.

REFERENCES

Axen, N., Hogmark, S., Jacobson, S., 2000. Friction and wear measurement techniques. In: Modern Tribology Handbook. CRC Press (Chapter 13).

Blatter, A., Maillat, M., Pimenov, S.M., Shafeev, G.A., Simakin, A.V., Loubnin, E.N., 1999. Lubricated sliding performance of laser-patterned sapphire. Wear 232, 226–230.

Dumitru, G., Romano, V., Weber, H.P., Haefke, H., Gerbig, Y., Pfluger, E., 2000. Laser microstructuring of steel surfaces for tribological applications. Appl. Phys. A: Mater. Sci. Process. 70, 485–487.

Dumitru, G., Romano, V., Weber, H.P., Pimenov, S., Kononenko, T., Hermann, J., Bruneau, S., Gerbig, Y., Shupegin, M., 2003. Laser treatment of tribological DLC films. Diam. Relat. Mater. 12, 1034–1040.

Kligerman, Y., Etsion, I., Shinkarenko, A., 2005. Improving tribological performance of piston rings by partial surface texturing. Trans. ASME 127, 632–638.

Kononenko, T.V., Pimenov, S.M., Konov, V.I., Romano, V., Bersos, B., Weber, H.P., 2000. Laser ablation and micropatterning of thin TiN coatings. Appl. Phys. A: Mater. Sci. Process. 71, 627–631.

Nakano, M., Korenaga, A., et al., 2007. Applying micro-texture to cast iron surfaces to reduce the friction coefficient under lubricated conditions. Tribol. Lett. 28, 131–137.

Nakano, M., Miyake, K., Korenaga, A., Sasaki, S., Ando, Y., 2007. Applying micro-texture to cast iron surfaces to reduce the friction coefficient under lubricated conditions. Tribol. Lett. 28, 131–137.

Pettersson, U., Jacobson, S., 2003. Influence of surface texture on boundary lubricated sliding contacts. Tribol. Int. 36, 857–864.

Pettersson, U., Jacobson, S., 2004. Friction and wear properties of micro textured DLC coated surfaces in boundary lubricated sliding. Tribol. Lett. 17, 553–559.

Pettersson, U., Jacobson, S., 2007. Texture surfces for improved lubrication at high pressure and low sliding speed of roller/piston in hydraulic motors. Tribol. Int. 40, 355–359.

Ryk, G., Kligerman, Y., Etsion, I., 2002. Experimental investigation of laser surface texturing for reciprocating automotive components. Tribol. Trans. 45, 444–449.

Saka, N., Tian, H., Suh, N.P., 1989. Boundry lubrication of undulated metal surfaces at elevated temperatures. Tribol. Trans. 32, 389–395.

SAS Institute Inc., 2008. SAS 9.2 software, help and documentation. Cary, NC.

Schurz, J., Ribitsch, V., 1987. Rheology of synovial fluid. Biorheology 24, 385–399.

Smith, A.F., 1985. The influence of surface oxidation and sliding speed on the unlubricated wear of 316 stainless steel at low load. Wear 105, 91–107.

Suh, N.P., 1981. The genesis of friction. Wear 69, 91–114.

Suh, N.P., Mosleh, M., Howard, P.S., 1994. Control of friction. Wear 175, 151–158.

Suh, N.P., Saka, N., 1987. Surface engineering. CIRP Ann. 36, 403–408.

Tian, H., Saka, N., Suh, Nam P., 1989. Boundry lubrication studies on undulated titanium surfaces. Tribol. Trans. 32, 289–296.

VanDamme, N.S., Wayman, B.H., Topoleski, L.D.T., 2003. Wear behavior of carbide coated Co–Cr–Mo implant alloy. J. Mater. Sci. Mater. Med. 14, 47–53.